# Calculation of the Magnetic Susceptibility from Susceptibility Weighted Phase Images

**A. Deistung[1], B. W. Lehr[1], F. Schweser[1], and J. R. Reichenbach[1]**

[1]Medical Physics Group, Institute for Diagnostic and Interventional Radiology, University Clinics, Friedrich-Schiller-University, Jena, Germany

***Introduction***

Magnetic susceptibility in MRI is a source of both contrasts and artefacts. For instance, susceptibility weighted phase images provide anatomical contrast complementary to the magnitude [1, 2] by directly reflecting local magnetic field changes induced by the distribution of magnetic susceptibility of the measured object. Therefore, quantitative mapping of the magnetic susceptibility could potentially enable a novel contrast for anatomic imaging and certain diagnoses that allow quantification of oxygen saturation in larger veins or estimation of local concentrations of contrast agents (e.g., cells labelled with superparamagnetic iron oxide particles (SPIOs)). An iterative method that enables quantitative mapping of the magnetic susceptibility for arbitrary shaped objects based on susceptibility weighted phase images was recently introduced by Morgan et al. [3]. In this paper we present modifications to this method that lead to an improved quality of the reconstructed susceptibility maps in vivo.

***Material and Methods***

**Theory:** Magnetic field $B_z$ and susceptibility $\chi$ are related via [4]: $\frac{1}{4\pi}\int_{K\neq r}\chi(r')\frac{3\cos^2\theta-1}{|r'-r|^3}d^3r' = \frac{B_z(r)-B_e(r)}{B_0} = RDF(r)$, where $B_z(r)$ is provided by the susceptibility weighted phase images, $B_e(r)$ is the background field, $B_0$ is the main magnetic field, $\theta$ is the angle between ***r*** and ***r'***, and the integration is evaluated over the region K. Discretizing the spatial domain the relative difference field (RDF) at position $r_i = (x(i), y(j), z(i))$ can be written in vector-matrix notation as: ***Ax***=***b***. The *N*x1 vector ***b*** concatenates *N* samples of the RDF, ***x*** contains *N*x1 samples of the susceptibility, and the *N*x*N* square matrix ***A*** contains the single voxel demagnetisation factors $A_{ij} = \frac{2(z(i)-z(j))^2-(x(i)-x(j))^2-(y(i)-y(j))^2}{4\pi\left[(x(i)-x(j))^2+(z(i)-z(j))^2+(y(i)-y(j))^2\right]^{5/2}}$ for $r_i \neq r_j$ and $A_{ij}=0$ for $r_j = r_i$. The matrix equation ***Ax***=***b*** can be solved using iterative solving algorithms, e.g., LSQR (Least-Squares using QR factorization) [3]. Since MRI does not provide reliable phase values in regions with no or low magnitude signal, the elements of ***b*** that correspond to these regions cannot be satisfied by ***x***. This may result in solution vectors ***x*** which are poor estimations of the true susceptibility distribution. Therefore, ***A*** was modified with a shutter-matrix ***S*** to allow arbitrary RDF-values in critical regions: ***SAx*** = ***b***. Furthermore, measured phase images contain a constant phase offset Δ***b*** (***b***=Δ***b***+***b*****0**) which may not be described by ***A***. In order to account for this offset an additional degree of freedom was added to the problem by expanding ***A*** with a row of ones yielding ***A''x'*** = ***b***. Accounting for both extensions the equation systems to be solved reduces to ***SA''x'***=***b***.

**Data acquisition data processing:** Volunteer data were acquired with a high-resolution 3D fully flow compensated gradient-echo sequence (TE/TR/FA = 20ms/30ms/15°, voxel size = 0.6×0.6×0.6mm³, 75% partial Fourier along phase and slice encoding direction) on a 3T MR-scanner (Tim Trio, Siemens Medical Solutions) using a 12-channel head-matrix coil. The multi-channel phase images were combined using uniform sensitivity reconstruction [5] and corrected using the freely available Phun-package [6]. Background field inhomogeneities $B_e(r)$ were estimated using the spherical mean value technique using a radius of 10px [4, 7].

***Results***

Figure 1 illustrates the steps of calculation from unwrapped phase images (Fig 1a) to the magnetic susceptibility (Fig 1e) in vivo. Solving the matrix equation **Ax**=**b** without shutter and offset induced low spatial frequencies superposed on the susceptibility map (Fig 1c). Although solving **SAx**=**b** reduced these slowly varying inhomogeneities, but high frequency artefacts still remained in the susceptibility map (Fig 1d). The susceptibility map computed with shutter and offset compensation (**SA''x'**=**b)** produced a nearly artefact free susceptibility image, However, small variations in susceptibility still occurred in the frontal brain. Extravascular field inhomogeneities in venous vessels were completely removed in the susceptibility map (see arrows in Fig 1). Another example shows that the susceptibility map accurately depicted the shape of the red nuclei (see arrows in Fig 2a and 2b) and compensates their field inhomogeneity in cranially located slices (Fig 2c and 2d).

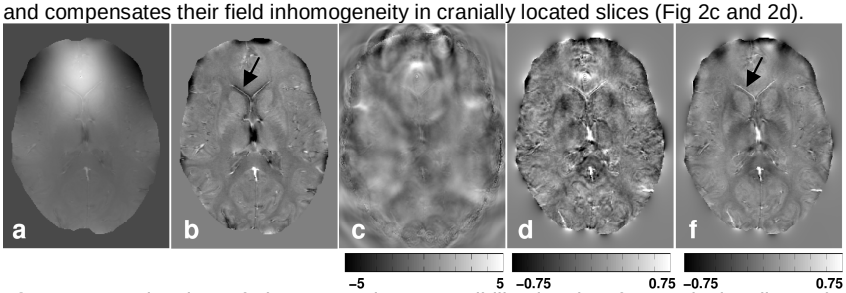


***Figure 1:*** *Estimation of the magnetic susceptibility in vivo for a single slice. The unwrapped phase image and RDF are shown in (a) and (b), respectively. The corresponding susceptibility maps were calculated without shutter (c), with shutter (d) as well as with shutter and offset (f).*

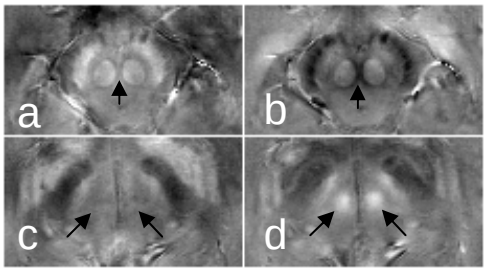


***Figure 2:*** *The susceptibility map (a, c) and its corresponding RDF (b, d) map show a slice at the location of the deep nuclei (top row) and a slice located 8mm cranially to (a).*

***Discussion***

We presented a method for calculation of the magnetic susceptibility *in vivo* by solving the linear equations with shutter and offset compensation. The field inhomogeneity pattern seen in phase images was efficiently removed in the susceptibility maps. In contrast to techniques that quantify magnetic susceptibility in Fourier domain [8, 9] the presented method overcomes problems with zeros in the denominator (of $\mathcal{F}(\chi(r))$) and, thus, requires only one single SWI scan without any rotations. The reliability of the values for magnetic susceptibility has to be evaluated in future studies using simulations and phantom measurements.

***References***

[1] Rauscher A et al. AJNR Am J Neuroradiol. 2005;26:736-42. [2] Deistung A et al. Magn Reson Med. 2008;60:1155-68. [3] Morgan J et al. In Proc ISMRM 2007. (abstract 35) [4] Li L et al. Magn Reson Med. 2004;51:1077-1082. [5] Ros C et al. In Proc ISMRM 2008. (abstract 1265) [6] Witoszynsky S et al. Medical Image Analysis. Epub. [7] Schweser F et al. submitted to ISMRM 2009. [8] Marques JP et al. Concepts Magn Reson B 2005;25: 65-78. [5] Schäfer et al. In Proc ISMRM 2008. (abstract 641).